ACS APPLIED MATERIALS & INTERFACES

Research Article

www.acsami.org

Fe-Species-Loaded Mesoporous MnO_2 Superstructural Requirements for Enhanced Catalysis

Ruting Huang,[†] Yanyu Liu,[†] Zhiwen Chen,*[,†,§] Dengyu Pan,[‡] Zhen Li,[†] Minghong Wu,*[,†,‡] Chan-Hung Shek,[§] C. M. Lawrence Wu,*[,§] and Joseph K. L. Lai[§]

[†]Shanghai Applied Radiation Institute and [‡]Institute of Nanochemistry and Nanobiology, School of Environmental and Chemical Engineering, Shanghai University, Shanghai 200444, People's Republic of China

[§]Department of Physics and Materials Science, City University of Hong Kong, Tat Chee Avenue, Kowloon Tong, Hong Kong

Supporting Information

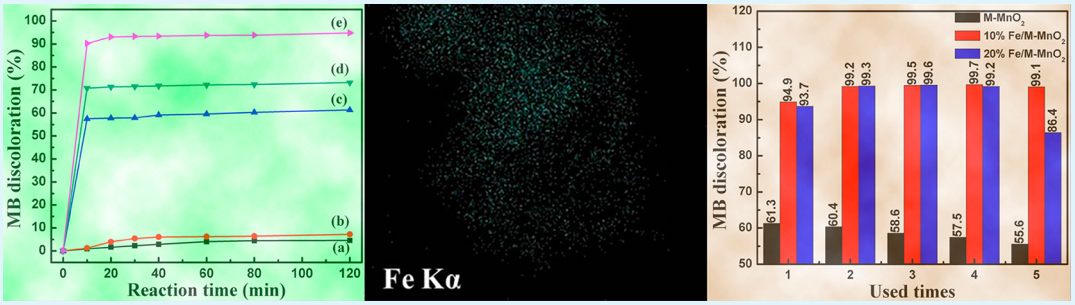

ABSTRACT: In this work, a novel catalyst, Fe-species-loaded mesoporous manganese dioxide (Fe/M-MnO_2) urchinlike superstructures, has been fabricated successfully in a two-step technique. First, mesoporous manganese dioxide (M-MnO_2) urchinlike superstructures have been synthesized by a facile method on a soft interface between CH_2Cl_2 and H_2O without templates. Then the M-MnO_2-immobilized iron oxide catalyst was obtained through wetness impregnation and calcination. Microstructural analysis indicated that the M-MnO_2 was composed of urchinlike hollow submicrospheres assembled by nanorod building blocks with rich mesoporosity. The Fe/M-MnO_2 retained the hollow submicrospheres, which were covered by hybridized composites with broken and shortened MnO_2 nanorods. Energy-dispersive X-ray microanalysis was used to determine the availability of Fe loading processes and the homogeneity of Fe in Fe/M-MnO_2. Catalytic performances of the M-MnO_2 and Fe/M-MnO_2 were evaluated in catalytic wet hydrogen peroxide oxidation of methylene blue (MB), a typical organic pollutant in dyeing wastewater. The catalytic degradation displayed highly efficient discoloration of MB when using the Fe/M-MnO_2 catalyst, e.g., ca. 94.8% of MB was decomposed when the reaction was conducted for 120 min. The remarkable stability of this Fe/M-MnO_2 catalyst in the reaction medium was confirmed by an iron leaching test and reuse experiments. Mechanism analysis revealed that the hydroxyl free radical was responsible for the removal of MB and catalyzed by M-MnO_2 and Fe/M-MnO_2. MB was transformed into small organic compounds and then further degraded into CO_2 and H_2O. The new insights obtained in this study will be beneficial for the practical applications of heterogeneous catalysts in wastewater treatments.

KEYWORDS: *MnO_2, mesoporous, superstructures, Fe-species-loaded MnO_2, enhanced catalysis*

1. INTRODUCTION

The dye industry is one of the most polluting in terms of volume and complexity of the organic pollutants. The wastewater from dye industries contains many organic pollutants, strong color, dissolved and suspended solids, etc. Degradation of refractory organic pollutants has attracted much attention in recent years because they can cause great harm to the natural environment and human health. Industrial dyes belong to one of the largest groups of pollutants.[1,2] These dyes usually have complex aromatic molecular structures which make them more recalcitrant to degrade. If not treated, these pollutants will induce certain health hazards such as carcinogenic risks and environmental contaminations.[3] The widespread occurrence of wastewater from dye industries, which amounts to more than seven million tons of approximately 10000 types annually produced worldwide, causes severe environmental problems.[4] Therefore, wastewater treatment of pollutants generated from dye processing industries poses a major challenge to the achievement of desired effluent discharge standards and to the proper recycle and reuse of these products in manufacturing processes.

Dyeing wastewater is generally refractory to conventional treatment techniques such as physical adsorption,[5] chemical oxidation, and biological methods.[6,7] Moreover, many problems resulting from the traditional methods, such as secondary pollution and retarded biodegradation of the accompanying

Received: September 3, 2014
Accepted: January 27, 2015
Published: January 27, 2015

DOI: 10.1021/am505989j
ACS Appl. Mater. Interfaces 2015, 7, 3949−3959

pollutants, are not avoided.[7] To develop a more efficient process for treating dyeing wastewater, advanced oxidation processes (AOPs), defined as those technologies that utilize the hydroxyl free radical (·OH) for oxidation in the presence of catalysts, have received increasing attention in the past decades. These processes, such as photocatalytic oxidation, Fenton's chemistry, and ozonation, have been applied successfully for the removal or degradation of recalcitrant pollutants, or used as pretreatment to convert pollutants into shorter-chain compounds that can then be treated by conventional or biological methods.[8] The classic example of AOPs is the Fenton reaction ($Fe^{2+} + H_2O_2 \rightarrow Fe^{3+} + OH^- + \cdot OH$), which is capable of degrading organic pollutants into harmless chemicals such as CO_2 and H_2O.[9] However, the application of the classical Fenton reagent, i.e., $Fe^{2+}/Fe^{3+}-H_2O_2$, is limited by the narrow working pH range (2−4) associated with this process and by separation and recovery of the iron species specific to industrial wastewater treatments.[10,11] Thus, some efforts have been made to develop heterogeneous Fenton systems which can be used over a wider pH range for the degradation of organic pollutants.[12] So far, many heterogeneous Fenton-like catalysts have been reported, such as iron oxides,[13,14] iron oxides immobilized on mesoporous silica,[15,16] and iron-pillared clays,[17,18] combined with carbon materials[19,20] or iron-containing ZSM-5.[21] Unfortunately, there are some problems in the case of heterogeneous catalysis. For example, the degradation reaction is relatively slow and inefficient at the range of neutral pH values because H_2O_2 decomposition is slow and only a small fraction of the H_2O_2 is converted into free radicals for degradation of recalcitrant contaminants.[15] Therefore, the search for proper active catalyst supports to prepare inexpensive, highly efficient, and stable heterogeneous catalysts for catalytic wet peroxide oxidation (CWPO) is of paramount importance.

Since the Fenton reaction involves an electron transfer process, transition metal oxides with accessible multiple oxidation states should have excellent catalytic performance.[9] Among various transition metal oxides, manganese dioxide (MnO_2) with different polymorphs, such as α-MnO_2, β-MnO_2, δ-MnO_2, γ-MnO_2, and ε-MnO_2, has been applied in the areas of catalysts, ion exchange, and electrochemical supercapacitors.[22] In particular, MnO_2 can be used as a heterogeneous catalyst for catalytic degradation of organic dyes.[22−25] Developing new materials with excellent catalytic performance depends not only on the multicomponents but also on the structural hierarchies of materials. Multicomponents and structural hierarchies are the key issues to realize multifunctional heterogeneous catalysts. Various micro/nanostructures of MnO_2, such as nanoparticles, nanorods, nanobelts, nanowires, nanotubes, nanofibers, nanosheets, mesoporous molecular sieves, branched structures, urchins/orchids, and other hierarchical structures, have been synthesized by different methods. However, mesoporous MnO_2 (M-MnO_2) has attracted significant interest because of their unique catalytic, electrochemical, magnetic, and adsorptive properties.[26−29] In recent years, the use of M-MnO_2, especially hierarchically structured M-MnO_2 self-assembled by nanostructures,[24,30,31] as catalysts, catalyst supports, adsorbents, and nanoreactors, has aroused enormous attention because of their widespread potential applications in catalysis. However, the environmental applications of M-MnO_2 for wastewater treatments are still in their infancy. If M-MnO_2 could be selected for catalyst supports to immobilize iron oxides, Mn and Fe species would be supplementary to each other in enhancing the catalytic capacity of catalysts in CWPO because Mn species can catalyze rapid H_2O_2 decomposition while Fe species urge it to produce more free radicals for the degradation of recalcitrant contaminants. Due to the similar atomic radius of Fe and Mn, Fe-substituted Mn may have some advantages, such as high degradation efficiency around neutral pH and easy recycle of catalysts in practical wastewater purification.[32] Therefore, the application of M-MnO_2-supported Fe catalysts in CWPO deserves investigation.

Herein, a novel catalyst, Fe-species-loaded mesoporous manganese dioxide (Fe/M-MnO_2) with urchinlike superstructures, has been fabricated successfully by a two-step technique. During the first step, the M-MnO_2 urchinlike superstructures have been synthesized by a facile method on a soft interface between CH_2Cl_2 and H_2O without templates. In the second step, the M-MnO_2 immobilized iron oxides through wetness impregnation and calcination to obtain the Fe/M-MnO_2 catalyst. Methylene blue (MB), a typical industrial pollutant in dyeing wastewater, was chosen as a model target contaminant to examine the catalytic performances of the M-MnO_2 and Fe/M-MnO_2. The stability of this Fe/M-MnO_2 catalyst in the reaction medium has been confirmed by the iron leaching test and reuse experiments. Quenching experiments of hydroxyl free radical (·OH) were carried out to investigate the possible reaction mechanism of the catalytic wet hydrogen peroxide oxidation of MB. These new insights obtained in this study are beneficial for the practical applications of heterogeneous catalysts in wastewater treatments.

2. EXPERIMENTAL SECTION

Synthesis of M-MnO_2. The method of preparing M-MnO_2 in this study is based on an improvement of previous works.[29,31] First, 30 mL of 1 M $MnSO_4$ solution was added into 80 mL of dichloromethane in a 200 mL beaker. After 5 min, the apparent H_2O/CH_2Cl_2 interface was obtained. Then 80 mL of 0.25 M $KMnO_4$ solution, through the CH_2Cl_2 layer at 30 drops/min controlled by a faucet of the dropping funnel, reached the CH_2Cl_2/H_2O interface along the tube of the funnel. During the reaction process, a brown material appeared at the interface and the whole $MnSO_4$ solution layer slowly turned brown. After 48 h, the brown products were collected by vacuum pumping filtration, washed three times with high-purity water and once with pure ethanol, and finally dried at 80 °C in air for 12 h. The sample obtained was denoted as M-MnO_2.

Fe-Loaded M-MnO_2 Catalysts. Fe-loaded M-MnO_2 catalysts were prepared by incipient wetness impregnation using $Fe(NO_3)_3 \cdot 9H_2O$ as iron precursor.[33] $Fe(NO_3)_3 \cdot 9H_2O$, needed for obtaining 10 wt % of iron in the final catalyst, was dissolved in high-purity water to get a desirable volume. The M-MnO_2 (0.9 g) was dispersed into the above solution under ultrasonic vibration for 30 min. The mixture was dried completely at 80 °C in air for 12 h, calcined in a muffle furnace in air from room temperature to 300 °C with a ramp rate of 5 °C/min, and kept at this temperature for 2 h. The obtained Fe-species-loaded M-MnO_2 catalyst was named Fe/M-MnO_2. In this work, the iron loading amount in the catalyst was 10 wt %. To find the difference between M-MnO_2 and Fe/M-MnO_2 in the catalytic degradation of methylene blue, the M-MnO_2 calcined in air at 300 °C for 2 h was also selected as the catalyst. In addition, the control experiment without adding M-MnO_2 was also conducted to verify the presence of iron oxide (Fe_2O_3) in the Fe loading process.

Catalytic Performances of Catalysts. The catalytic performances of the obtained catalysts were evaluated in the catalytic oxidation of methylene blue (MB) as described in detail in the following. These catalysts were dried at 110 °C for 10 h to eliminate moisture beforehand. First, 100 mL of the MB dye solution (100 mg/L) and 20 mL of the H_2O_2 solution (30 wt %) were combined in a 250 mL glass flask, and then the catalytic reaction was started by the addition of 50

DOI: 10.1021/am505989j
ACS Appl. Mater. Interfaces 2015, 7, 3949−3959

mg of the catalysts to the flask, which was considered the initial instant of reaction (t = 0). The reactor was located in a shaking incubator (constant temperature about 25 °C, 100 r/min, and atmospheric pressure). For a given time interval, 2 mL of the mixture solution was pipetted into a centrifuge tube with 0.5 mL of *tert*-butyl alcohol and quickly diluted with distilled water to 20 mL. The diluted solution was immediately centrifuged (rotating speed at 3500 r/min for 5 min) to remove the catalyst particles. The supernatant was then put into a quartz cell (path length 1.0 cm), and the absorbance was measured with a double-beam ultraviolet−visible (UV−vis) spectrophotometer (TU-1901, Beijing Puxi Universal Apparatus Co Ltd., China) at 664 nm (characteristic wavelength of methylene blue). The pH of the reaction solution was also successively measured during the reaction. Along the reaction, the solution pH remained almost unchangeable in a small range of 6−7. When the reaction time reached 120 min, the solution in the flask was centrifuged with a rotating speed of 3500 r/min for 10 min. The supernatant was used for the chemical oxygen demand (COD) experiment, total organic carbon (TOC) measurement, and metal ion leaching tests. The COD experiment was conducted according to the fast digestion spectrophotometric method (HJ/T 399-2007, China). The TOC concentration in the reaction solution was determined using an Analytikjena TOC/TN analyzer (multi N/C 2100, Analytik Jena AG, Germany). The concentration of Fe and Mn in the solution was determined by an inductive coupled plasma atomic emission spectrometer (ICP-AES, 2A051657, Leman Laboratories Inc., Arlington, VA). The catalyst stability was also investigated through reuse experiments using the standard oxidation conditions. In a typical test, 25 mg of the catalysts was placed in contact with 50 mL of methylene blue solution (100 mg/L) and 10 mL of the H_2O_2 solution (30 wt %) under stirring for 2 h. The catalysts were then centrifuged (rotating speed at 3500 r/min for 10 min) and collected for the next oxidation cycle, maintaining the same standard proportions. A MB degradation rate of 120 min as a function of reuse time of the catalyst was selected as an index to investigate the possibility of recycling the catalysts. Used chemicals, catalyst characterizations, and catalytic performances of filtered solutions in this study are described in detail in the Supporting Information.

3. RESULTS AND DISCUSSION

Catalyst Compositions. Figure 1 shows the powder X-ray diffraction (XRD) patterns of the as-synthesized samples: (a) M-MnO_2, (b) 10 wt % Fe/M-MnO_2, (c) the control sample (Fe_2O_3) prepared under same condition without adding M-MnO_2. As seen from the wide-angle pattern of M-MnO_2 (Figure 1a), there are obvious diffraction peaks at 2θ = 37.0°, 42.2°, 55.9°, and 66.1°, which can be easily identified for the

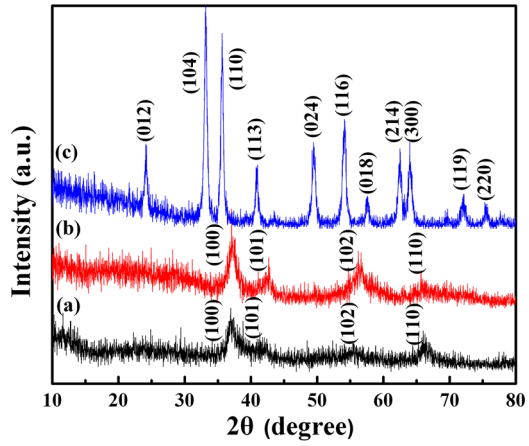

Figure 1. XRD patterns of the as-synthesized samples: (a) M-MnO_2, (b) 10 wt % Fe/M-MnO_2, (c) the control sample (Fe_2O_3) prepared under same condition without adding M-MnO_2.

(100), (101), (102), and (110) planes of the ε-MnO_2 crystalline structure (Akhtenskite, syn MnO_2, JCPDS, no. 30-0820). The crystal phase of the as-synthesized MnO_2 sample in this study is different from that presented in previous reports.[29,31] This is attributed to the difference in reagents and soft interfaces. All diffraction peaks of the MnO_2 samples are broad and weak owing to the poor crystallinity or the small crystal domain in the products, which resulted from the low preparation temperature.[34] Figure 1c reflects the fact that $Fe(NO_3)_3$ decomposed into α-Fe_2O_3 (hematite, syn Fe_2O_3, JCPDS, no. 33-0664) after calcination at 300 °C for 2 h. Compared with M-MnO_2, the XRD patterns of 10 wt % Fe/M-MnO_2 (Figure 1b) have no obvious new peak in the absence of the peak at 2θ = 33° indexed to α-Fe_2O_3, which is different from that of Zhang's report.[33] On the contrary, a similar type of behavior has been reported by Dubal and co-workers[35,36] for Fe-doped MnO_2 thin films grown on stainless steel substrates. They explain that the remaining peaks observed in the XRD patterns are due to stainless steel substrates. Perhaps, it was thought that the lack of peak assignment to iron species in 10 wt % Fe/M-MnO_2 should be ascribed to their low contents and high dispersion. However, there are always no peaks assigned to iron species in Fe/M-MnO_2 at different Fe concentrations ranging from 5 to 30 wt % (Figure S1), which is contrary to the above suggestion. Careful observations indicated that the diffraction peaks of Fe/M-MnO_2 have slight right deviation. For example, the XRD peaks of 10 wt % Fe/M-MnO_2 (Figure 1b) appeared at 2θ = 37.1°, 42.5°, 56.1°, and 66.6°. This study proposes a new explanation for the phenomenon observed in the XRD patterns. Generally speaking, the occurrence of atomic replacement in the lattice will cause a change in the lattice parameter. With the same number of electronic shells, the atomic radius of iron ion (Fe^{3+}) is smaller than that of manganese ion (Mn^{4+}). According to the Bragg equation, the XRD peaks shift slightly to larger angle when the radius of the replacement atom is smaller than that of the previous atom in the lattice. The characteristic peaks of iron oxides did not appear in the XRD patterns of Fe/M-MnO_2. Since Fe is implanted after the MnO_2 lattice is formed through insipient wetness and sonication, the sonication provided the necessary energy to break a Mn−O bond and aliovalently substitute Fe^{3+}. This phenomenon has also been observed in previous literature.[37−40] It can be inferred that Fe replaces Mn in the MnO_2 lattice without a large change in lattice parameter. In brief, Fe/M-MnO_2 can be regarded as the hybridized composite.

The above observation can be further investigated by Fourier transform infrared (FTIR) spectra of the M-MnO_2 and 10 wt % Fe/M-MnO_2 (Figure S2, Supporting Information). As observed in Figure S2, the broad peak at 3382 cm^{-1} is due to the presence of a silanol group or a OH group of an adsorbed water molecule. Several small peaks in the range of 1400−1650 cm^{-1} are found to correspond to bending vibrations of water molecules and hydroxyl groups combined with metal atoms.[22,41] The results are due to the fact that the M-MnO_2 synthesized in aqueous solution may form a tunnel structure during the reaction process; thus, some H_2O molecules are intercalated in the tunnel.[35] The M-MnO_2 and Fe/M-MnO_2 show major peaks at 500−600 cm^{-1} which arise from the stretching vibration of the Mn−O and Mn−O−Mn bonds in [MnO_6] octahedral.[35,42] The FTIR spectra of the M-MnO_2 and Fe/M-MnO_2 are similar. The peaks associated with the vibrations of Mn−O bonds are slightly shifted after Fe loading.

DOI: 10.1021/am505989j
ACS Appl. Mater. Interfaces 2015, 7, 3949−3959

This confirms that Fe may replace the position of Mn in the MnO_2 lattice without significant lattice distortion.

Figure 2 presents the (a) transmission electron microscopy (TEM) micrograph of 10 wt % Fe/M-MnO_2 as well as

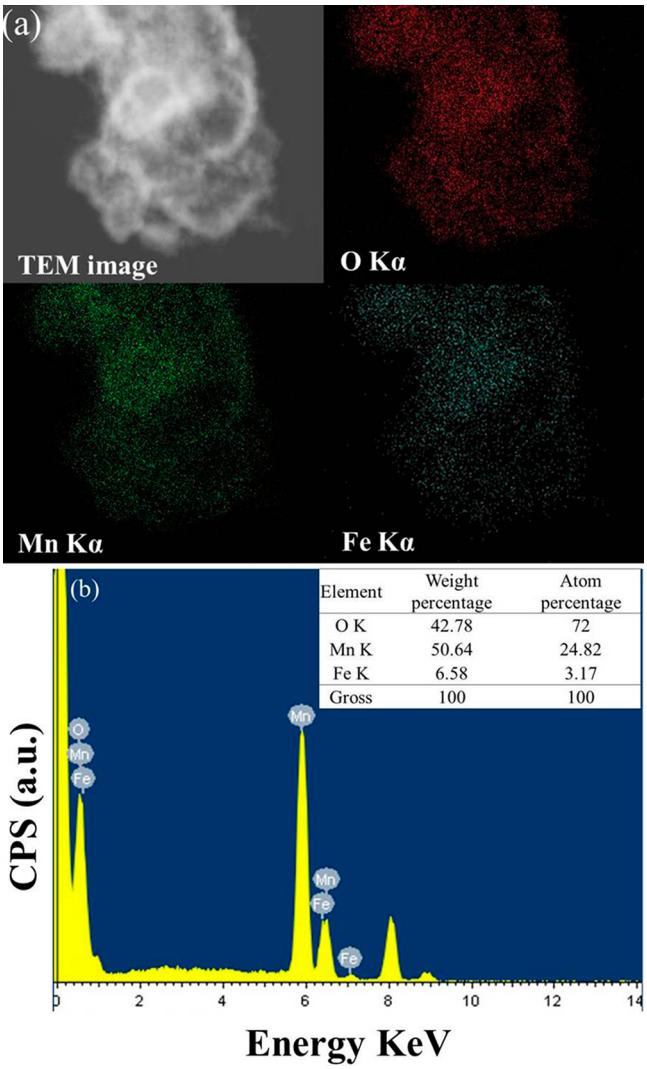

Figure 2. (a) TEM micrograph of 10 wt % Fe/M-MnO_2 as well as elemental mapping of the O (red zone), Mn (green zone), and Fe (blue zone). (b) EDXS microanalysis spectrum with the inset showing the results of elemental analysis.

elemental mapping of O (red zone), Mn (green zone), and Fe (blue zone) and the (b) energy dispersive X-ray (EDX) microanalysis spectrum with the inset showing the results of elemental analysis. Elemental analysis clearly shows the homogeneity of Fe in Fe/M-MnO_2, which further proves that the Fe/M-MnO_2 is a hybridized composite instead of a mixture of iron and manganese oxides. O, Mn, and Fe were also found in EDX spectrometry (EDXS) measurements as shown in Figure 2b, which confirms the presence of Fe, Mn and O in Fe/M-MnO_2.[35] The average percentage of O, Mn, and Fe are listed in the inset of Figure 2b. The elemental composition analysis determined that only 6.58 wt % Fe has been loaded in Fe/M-MnO_2, which agrees with Fe content (7.14 wt %) detected by inductively coupled plasma-atomic emission spectrometry (ICP-AES). A similar phenomenon has been reported by Martinez et al.[43] Water molecules and hydroxyl groups combined with Mn atoms resulted in a higher content of O, whose atomic concentration was about twice that of metal atoms in 10 wt % Fe/M-MnO_2. Thus, the lower than 10 wt % content of Fe is related to the partial loss of $Fe(NO_3)_3$ in the loading process.

Morphology and Microstructure. The morphologies and microstructures of the obtained M-MnO_2 and 10 wt % Fe/M-MnO_2 were examined by scanning electron microscopy (SEM, Figure S3, Supporting Information) and TEM. As seen from the higher-magnification SEM images of M-MnO_2 (Figure S3a, right) and 10 wt % Fe/M-MnO_2 (Figure S3b, right), the panoramic morphologies are composed of numerous submicrospheres with thorns on the surface. Figure 3 shows the TEM

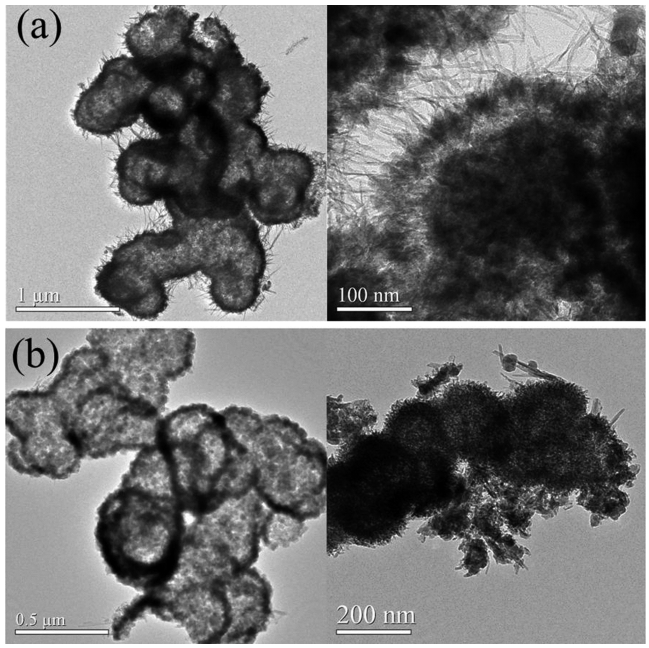

Figure 3. TEM images of (a) M-MnO_2 and (b) 10 wt % Fe/M-MnO_2 at different magnifications.

images of M-MnO_2 (Figure 3a) and 10 wt % Fe/M-MnO_2 (Figure 3b) at different magnifications. The two samples consist of hollow urchins with visible interior cavities. A few spheres with surface damage are observed in Figure 3a, which confirms that the as-synthesized MnO_2 submicrospheres have a hollow structure. Microstructure analysis indicates that the M-MnO_2 has uniform submicrospheres with size ranges from 200 to 500 nm. Contrary to literature reports,[23,29,31] the as-synthesized submicrospheres in this study have smaller diameter, which can be ascribed to the different thicknesses of the soft interface. The higher-magnification TEM image of M-MnO_2 shown in Figure 3a (right) offers a clear view of the surface microstructure, which exhibits urchinlike hierarchical MnO_2 submicrospheres composed of numerous compact nanorods growing in all directions. This further reveals that the as-prepared submicrospheres were assembled from numerous one-dimensional MnO_2 nanorod building blocks with rich mesoporosity. Careful consideration of the higher-magnification TEM image reveals that mesopores also exist in the gaps between two submicrospheres. The TEM images shown in Figure 3b clearly demonstrate the fact that the Fe/M-MnO_2 retains the hollow submicrospheres, which are covered

DOI: 10.1021/am505989j
ACS Appl. Mater. Interfaces 2015, 7, 3949−3959

by hybridized composites with broken and shortened MnO_2 nanorods.

Porous Properties. Figure 4 shows the nitrogen adsorption−desorption isotherms (Figure 4a) and pore-size

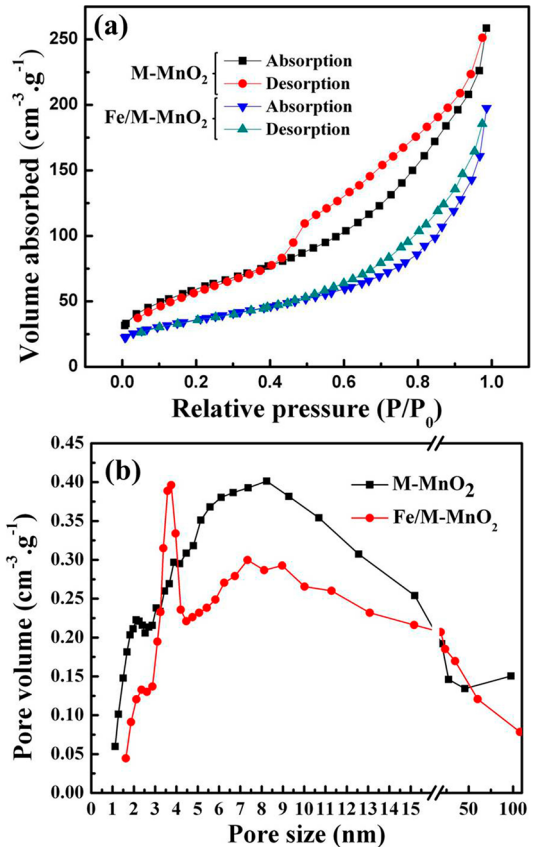

Figure 4. N_2 adsorption−desorption isotherms (a) and pore size distribution (b) of M-MnO_2 and 10 wt % Fe/M-MnO_2.

distributions (Figure 4b) of M-MnO_2 and 10 wt % Fe/M-MnO_2. The N_2 adsorption−desorption isotherms shown in Figure 4a can be classified as type IV according to IUPAC (International Union of Pure and Applied Chemistry) classification.[44] A distinct type H3 hysteresis loop in the larger range of 0.45−1.00 P/P_0 can be observed in the adsorption−desorption isotherms of M-MnO_2, providing more evidence for mesoporous MnO_2 structure. The type H3 hysteresis loop demonstrates that this sample consists of particles or split-shape materials, which implies that the M-MnO_2 should possess hierarchical porosity. This deduction can be further supported by the pore-size distributions of M-MnO_2 shown in Figure 4b. The pore sizes of M-MnO_2 are distributed in the range 1.3−100 nm, with the majority clustering in the range 1.3−15 nm. The smaller diameter ones are in the range 1.5−2.5 nm, and the larger diameter ones are in the range 5−10 nm. The hierarchical porosity should be ascribed to the mesopores between submicrospheres and the mesopores existing in the one-dimensional MnO_2 nanorod building blocks. The pores in this study are smaller and more uniform than those of the hierarchical mesoporous materials reported by previous workers.[23,29,45] In Fe-species-loaded M-MnO_2 urchinlike superstructures, the incorporation of Fe into the walls of M-MnO_2 results in a significant effect on the textural properties of this composite. The Fe/M-MnO_2 exhibits a H4 type broad hysteresis loop, which is also typical of split-shape mesoporous materials. As the relative pressure increases, two isotherms exhibit a sharp step characteristic of capillary condensation of nitrogen within uniform mesopores, where the P/P_0 position of the inflection point correlates with the diameter of mesopore.[25] The P/P_0 position of the inflection point corresponding to Fe/M-MnO_2 is located at a higher relative pressure compared to that of M-MnO_2 (Figure 4a), which reflects the larger mesopores of Fe/M-MnO_2. This conclusion is also supported by the pore size distribution of M-MnO_2 and Fe/M-MnO_2 (Figure 4b). The measured average pore diameters of M-MnO_2 and Fe/M-MnO_2 are 5.87 and 6.85 nm, respectively (Table S1, Supporting Information). It is worth noting that the peak pore diameter of Fe/M-MnO_2 (3.58 nm) was larger than that of M-MnO_2 (1.82 nm), which supports the viewpoint that the nanorods have been damaged and the gap mesopores became larger owing to the loading of Fe. After the loading of Fe, the specific surface area declined from 219.3 to 129.1 $m^2 \cdot g^{-1}$ and the pore volume decreased from 0.451 to 0.355 $cm^3 \cdot g^{-1}$ (Table S1, Supporting Information). The above evidence points to Fe, which is implanted as an iron oxide on the surface, having a drastic effect on pore size and volume even if Fe inclusion into the crystal structure does not have such a drastic effect on the porosity. This is due to the blocking of some micropores or mesoporous channels by iron oxide. The reduction of textural properties due to Fe loading has also been observed in metal-immobilized SBA-15 and activated carbon materials.[20,46]

Catalytic Properties of M-MnO_2 and Fe/M-MnO_2. The obtained M-MnO_2 and Fe/M-MnO_2 urchinlike hierarchical superstructures would be expected to show superior surface-related properties such as catalytic performance, because of their vast specific surface area. To examine catalytic properties of M-MnO_2 and Fe/M-MnO_2 as a means of generating free radicals for degradation of organic matter, methylene blue (MB) as a typical industrial pollutant in wastewater was chosen for discoloration. The oxidative degradation of the MB solution (100 mg/L) under near-neutral pH was conducted by using H_2O_2 as oxidant (1.12 g/mL) and M-MnO_2 and Fe/M-MnO_2 as catalysts (0.50 g/L).

Discoloration Efficiency of MB Solution. In general, the discoloration efficiency of the MB molecules (denoted as r) was calculated as follows:

$$r = \frac{C_0 - C}{C_0} = \frac{A_0 - A}{A_0}$$

(when dilution multiple was the same)

where C_0 ($g \cdot L^{-1}$) is the initial concentration of the mixture of MB and H_2O_2 solutions, C ($g \cdot L^{-1}$) is the concentration of the mixture solution at different intervals during the reaction, A_0 is the absorbance of the mixture solution at 664 nm at t = 0 min, and A is the absorbance at the same wavelength at a given reaction time. Considering the volume change of the solution when H_2O_2 solution was added, the solution mixture of 50 mL of MB and 10 mL of H_2O was selected as the initial solution at t = 0 min in this study. As shown in Figure 5, line a indicates that the Fe/M-MnO_2 adsorbs a little MB from the solution, in agreement with previous results reported in the literature.[2,33] The characteristic feature is to provide a large amount of active sites derived from Fe/M-MnO_2, which catalyzes H_2O_2 decomposition to generate free radicals. Line b demonstrates that only ca. 7.2% of MB is decomposed without any catalyst even after reacting for 120 min. No obvious discoloration is

DOI: 10.1021/am505989j
ACS Appl. Mater. Interfaces 2015, 7, 3949−3959

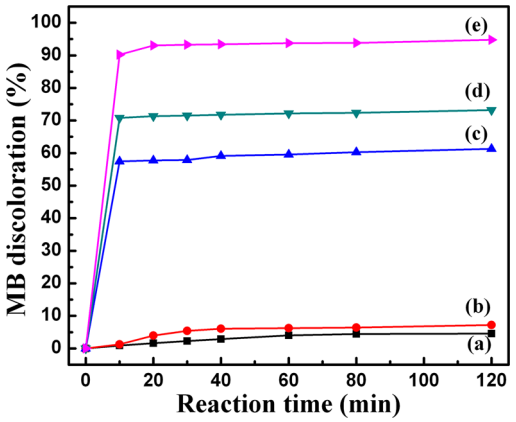

Figure 5. Discoloration rates of the MB using H_2O_2 as oxidant and different catalysts: (a) 10 wt % Fe/M-MnO_2 + MB without H_2O_2, (b) MB + H_2O_2 without catalyst, (c) M-MnO_2 + MB + H_2O_2, (d) the calcined M-MnO_2 + MB + H_2O_2, and (e) 10 wt % Fe/M-MnO_2 + MB + H_2O_2. Error bar = 0.3%.

observed in Figure 5a,b when there is no H_2O_2 or catalysts. Therefore, it can be declared here that the degradation of MB molecules is caused by H_2O_2-induced oxidation catalyzed by catalysts. It can be seen that ca. 61.3% of MB can be decomposed in 120 min using M-MnO_2 as catalyst as shown in Figure 5c. About 90.2% of MB is decomposed within 10 min in the presence of Fe/M-MnO_2 as catalyst as shown in Figure 5e, which demonstrates that the catalytic reaction occurred rapidly. This result is ascribed to the rapid H_2O_2 decomposition catalyzed by Fe/M-MnO_2. When the decomposition reaction was conducted for 120 min, ca. 94.8% of MB was decomposed. Obviously, the catalytic activity of Fe/M-MnO_2 is much higher and faster than that of M-MnO_2. As a comparison, the M-MnO_2 is subjected to calcination. Although the calcined M-MnO_2 (with the same weight, e.g., 50 mg) also exhibits higher catalytic performances (Figure 5d) than as-synthesized M-MnO_2 with an increase of 10% in the degradation of MB, it is also weaker than the Fe/M-MnO_2 in catalyzing H_2O_2 to generate free radicals for the degradation of MB. The elevated efficiency of the calcined M-MnO_2 is ascribed to better crystallinity and a cleaner catalyst surface.[22] Interestingly, the Fe loading significantly improves the catalytic performances of M-MnO_2. The excellent catalytic performance of the Fe/M-MnO_2 appears to confirm the hypothesis that the iron oxides enhance H_2O_2 decomposition catalyzed by M-MnO_2 to generate more free radicals.

However, catalytic performance described only by the conversion degree of MB is unconvincing and inappropriate because both the catalytic capacity of the catalyst and H_2O_2 consumption are responsible for the removal of MB. Since H_2O_2 is always totally consumed in the catalytic reaction, the catalytic performance of catalyst should be estimated by the following equation:

$$q = \frac{(C_0 - C)V_0}{VW} = \frac{M_0 \times r}{VW}$$

where q ($g{\cdot}L^{-1}{\cdot}g^{-1}$) is the consumption of MB caused by 1 g of catalyst and 1 L of 30 wt % H_2O_2 solution, C_0 ($g{\cdot}L^{-1}$) has the same meaning as above but C ($g{\cdot}L^{-1}$) is the concentration of the mixture solution at 120 min. V_0 (L) is the initial volume of the mixture, i.e., 120 mL, V (L) is the volume of a 30 wt % H_2O_2 solution added to the MB solution, i.e., 20 mL, W (g) is the weight of the catalyst, i.e., 0.050 g, and M_0 (g) means the initial mass of MB. The q of M-MnO_2 in this study is ca. 12.26 $g{\cdot}L^{-1}{\cdot}g^{-1}$, which is more effective than ca. 3.20 $g{\cdot}L^{-1}{\cdot}g^{-1}$ of β-MnO_2 hollow octahedral,[24] ca. 2.46 and 8.13 $g{\cdot}L^{-1}{\cdot}g^{-1}$ of β-MnO_2 nanorods,[2,25] and ca. 6.67 $g{\cdot}L^{-1}{\cdot}g^{-1}$ of MnO_2 nanofiber.[1] This better catalytic performance of M-MnO_2 is due to the urchinlike hierarchical MnO_2 submicrospherical superstructure. The q value of 10 wt % Fe/M-MnO_2 is ca. 18.96 $g{\cdot}L^{-1}{\cdot}g^{-1}$, which is higher than 12 $g{\cdot}L^{-1}{\cdot}g^{-1}$ of iron oxide dispersed over activated carbon (ACK/Fe),[47] ca. 3 $g{\cdot}L^{-1}{\cdot}g^{-1}$ of titanomagnetite ($Fe_{3-x}Ti_xO_4$),[48] and ca. 2.16 $g{\cdot}L^{-1}{\cdot}g^{-1}$ of graphene oxide with organo-building blocks of Fe-aminoclay.[18] In contrast to iron oxide dispersed into other supports,[19,21,48] the highlight of Fe/M-MnO_2 is that the H_2O_2 decomposition and MB degradation are both very rapid, which is ascribed to the catalytic performances of the M-MnO_2 support toward H_2O_2 decomposition.

Degradation Degree of MB Solution. The temporal evolutions of MB solution under catalysis from 10 wt % Fe/M-MnO_2 were monitored with ultraviolet−visible (UV−vis) spectrometry (Figure S4, Supporting Information). After 10 wt % Fe/M-MnO_2 was added, the intensities of the characteristic peaks of MB at 614 and 664 nm decreased rapidly within 10 min. With further elapse of reaction time, the decrease in MB peaks continued but much more slowly. Moreover, the bands at 614 and 664 nm became very broad and weak. At the same time, the color of the mixture turned shallow gray and finally became colorless. The original absorption maximum at 664 nm shifted to 640 nm after reaction for 10 min. The obvious blue shift of the absorption band indicated the catalytic degradation of MB.[9]

Even though an obvious discoloration of the MB solution was observed within 2 h reaction (Figure 5), these data cannot give satisfactory results for MB degradation. The mineralization processes can transform soluble organic intermediates to CO_2 and H_2O. In fact, the total mineralization of an organic compound such as MB containing C, S, and N functions leads generally to the formation of CO_2, SO_4^{2-}, NH_4^+ and/or NO_3^-.[45] Besides the discoloration, the mineralization of MB solution should be given close attention from the viewpoint of the industrial wastewater treatments.[50] To gain insights into the degradation degree of MB, chemical oxygen demand (COD) and total organic carbon (TOC) analyses should be conducted to evaluate the decontamination of all residual carbon-containing metabolites. The related data are shown in Table 1. The COD and TOC removals show ascent when Fe loading content increases, indicating that the Fe loading contributes to MB mineralization. The COD and TOC removal rate of MB solution under catalysis from 10 wt % Fe/M-MnO_2 are both about 19%, which indicates that the MB is transformed into soluble organic intermediates instead of undergoing complete

Table 1. Degradation Degrees of the MB Solution Catalyzed by M-MnO_2 and Fe/M-MnO_2

	COD (mg/L)	COD removal (%)	TOC (mg/L)	TOC removal (%)
MB solution	190 ± 2	–	46 ± 2	–
M-MnO_2	172 ± 2	9.5 ± 0.5	40 ± 2	13.0 ± 0.5
10% Fe/M-MnO_2	154 ± 2	19.0 ± 0.5	37 ± 2	19.6 ± 0.5
20% Fe/M-MnO_2	142 ± 2	25.3 ± 0.5	35 ± 2	23.9 ± 0.5

DOI: 10.1021/am505989j
ACS Appl. Mater. Interfaces 2015, 7, 3949−3959

mineralization.[50] Although no specific new UV−vis peak was observed in the spectra of MB solution under catalysis from 10 wt % Fe/M-MnO_2 (Figure S4, Supporting Information), the TOC in the solution still remained as high as 81%. This contradiction indicates that the MB is degraded to small organic compounds that are not detected by UV−vis spectrometry. Similar phenomenon has also been reported in the literature.[51] This result reflects that Fe/M-MnO_2 effectively decolorizes MB but does not completely decompose the dye into CO_2 and H_2O.

Stability Test of M-MnO_2 and Fe/M-MnO_2. The stability of catalysts is crucial to their application during catalytic processes. Herein, the discoloration of the MB solution in 120 min as a function of the number of reuse times using different catalysts was investigated, and the results are shown in Figure 6.

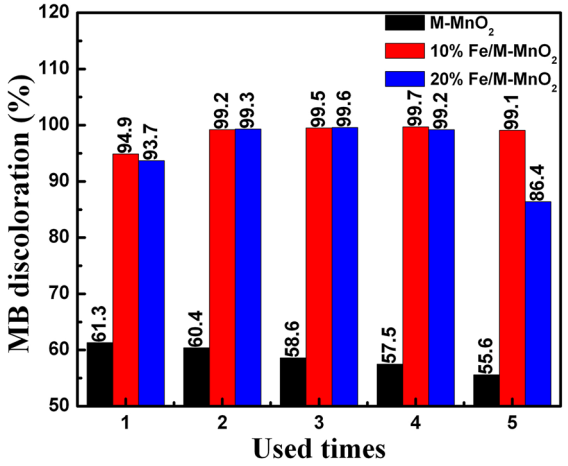

Figure 6. MB discoloration in 120 min as a function of reuse times of the catalysts. Error bar = 0.3%.

The catalytic capacity of M-MnO_2 shows a slight decrease with the increase of the number of use times, which results in the loss of catalyst and damage to the hierarchical M-MnO_2 superstructures. Compared with M-MnO_2, the catalytic capacity of Fe/M-MnO_2 ascends initially to a certain number of use times and then descends gradually. The discoloration rate of the MB catalyzed by 10 wt % Fe/M-MnO_2 arrived at the maximum at the fourth time. However, the maximum corresponding to 20 wt % Fe/M-MnO_2 was obtained at the third time. Why does this strange phenomenon appear? This is due to the different losses of Mn and Fe species in the reaction medium as shown in Table 2. Mn species in Fe/M-MnO_2 is a crucial factor for the velocity of H_2O_2 decomposition while Fe species in Fe/M-MnO_2 urge H_2O_2 to produce more free radicals. Mn and Fe species are supplementary to each other in the catalytic wet peroxide oxidation of MB solution. Because the leaching content of Mn in mixed solution is much larger than that of Fe as shown in Table 2, the ratio of Fe to Mn atoms on the surface of the urchinlike MnO_2 submicrospheres is increasing gradually. Consequently, the catalytic capacity of Fe/M-MnO_2 for generating free radicals is strengthened but the rate of H_2O_2 decomposition declines. This conclusion can also be supported by the experimental phenomenon that the time of bubble production is prolonged with the increase in the number of use times. Although the reaction time was 120 min, tiny bubbles were produced at the fifth time of the MB degradation experiment catalyzed by Fe/M-MnO_2. This shows that the reaction is continuing. Therefore, the change of MB discoloration percentage in 120 min as a function of the number of reuse times using Fe/M-MnO_2 as catalyst derives mainly from the change of Fe/Mn ratio on the surface of Fe/M-MnO_2 submicrospheres.

Table 2. Stability of the Metal Species in the Catalysts

catalysts	$[Mn]_{deflected}$ (ppm)	$[Mn]_{lost}$ (%)	$[Fe]_{deflected}$ (ppm)	$[Fe]_{lost}$ (%)
M-MnO_2	11.3 ± 0.5	3.6 ± 0.3	–	–
10% Fe/M-MnO_2	31.4 ± 0.5	11.1 ± 0.3	0.11 ± 0.5	0.6 ± 0.3
20% Fe/M-MnO_2	33.4 ± 0.5	13.2 ± 0.3	0.29 ± 0.5	0.8 ± 0.3

Another important point in the oxidation process that involves a heterogeneous catalyst is the stability of the active species during the reaction.[52] The dissolubility of Mn and Fe species in solution is also selected as an index to assess the catalytic stability of the catalyst. Table 2 shows the concentration of Mn and Fe species in the reaction medium in the presence of different catalysts. The concentration of Mn ions in mixed solution in catalysis from M-MnO_2 is 11.3 mg/L while the concentration of Mn ions in mixed solution under catalysis from Fe/M-MnO_2 is nearly three times as much as that of M-MnO_2. The increase of Mn loss is ascribed to the situation that the Fe replaces Mn in MnO_2 lattice and new dissoluble Mn species form on the surface of Fe/M-MnO_2 submicrospheres. This deduction is further supported by the contrast of 10 wt % and 20 wt % Fe/M-MnO_2. The Mn and Fe loss from 20 wt % Fe/M-MnO_2 are both little more than those of 10 wt % Fe/M-MnO_2. The Fe loss from Fe/M-MnO_2 in the reaction medium seems to be too small for consideration. The above metal iron leaching tests indicate the remarkable stability of the prepared Fe/M-MnO_2 composites in the reaction medium.

Reaction Mechanism. The low concentrations of dissolved Fe and Mn shown in Table 2 indicate that the whole decomposition process is a heterogeneous Fenton reaction. To further verify this conclusion, the solutions in reusability experiments are filtered to remove the solid catalysts and used as the catalyst for the CWPO of MB solution. The corresponding discoloration efficiencies for MB solution are shown in Table 3. The filtered solutions of M-MnO_2 + H_2O_2 + MB system, 10 wt % Fe/M-MnO_2 + H_2O_2 + MB system, and 20 wt % Fe/M-MnO_2 + H_2O_2 + MB system at the first time, 20 wt % Fe/M-MnO_2 + H_2O_2 + MB system at the second time, are designated as C1, C2, C3, C3-2, respectively (see Supporting Information). The MB discoloration efficiency grows with increasing Fe concentration in the filtered solution, but the maximum discoloration is merely 9%, indicating that the catalytic performance of the filtered solution is very poor. In contrast to the corresponding catalysts described in Figure 6, it is easy to conclude that the M-MnO_2 + H_2O_2 + MB system and

Table 3. Catalytic Performances of the Filtered Solutions in the M-MnO_2 + H_2O_2 + MB System and Fe/M-MnO_2 + H_2O_2 + MB System

catalysts	C1	C2	C3	C3−2
MB degradation	1.2 ± 0.3%	3.1 ± 0.3%	5.3 ± 0.3%	9.0 ± 0.3%

DOI: 10.1021/am505989j
ACS Appl. Mater. Interfaces 2015, 7, 3949−3959

Fe/M-MnO_2 + H_2O_2 + MB system are both heterogeneous catalytic systems instead of homogeneous catalytic systems.

Further development of the Fe/M-MnO_2 composites requires a clear understanding of the oxidative degradation mechanism of MB with H_2O_2 as oxidant. Zhang et al. confirmed that the destructive oxidation of MB occurs on or near the catalyst surface whereby the in situ-produced free radical species (e.g., ·OH, HOO·, or $O_2\cdot^-$) rather than O_2 serve as oxidizing agents.[2] Herein, the quenching experiment for ·OH is conducted to confirm the presence of ·OH in the reaction medium. Three milliliters of 98 wt % *tert*-butyl alcohol, a strong radical scavenger (the reaction rate with hydroxyl radicals is $3.8-7.6 \times 10^8$ M^{-1} s^{1-}),[53,54] is added into the solution mixture of MB (50 mL, 100 mg/L) and the catalysts (25 mg of M-MnO_2 or Fe/M-MnO_2) before adding H_2O_2 solution (10 mL, 30%) and then reacted for 60 min under controlled pH = 6−7 and temperature T = 25 °C. Figure 7 indicates that the MB discoloration is markedly inhibited by *tert*-butyl alcohol, indicating that the hydroxyl free radicals are mainly responsible for the removal of MB. The addition of *tert*-butyl alcohol markedly reduced the removal efficiency of MB in M-MnO_2 + H_2O_2 + MB system with a decrease of 43.9% while the decrement of MB removal in Fe/M-MnO_2 + H_2O_2 + MB system was 31.7%, suggesting the Fe/M-MnO_2 accelerated the H_2O_2 transformation into ·OH free radicals.

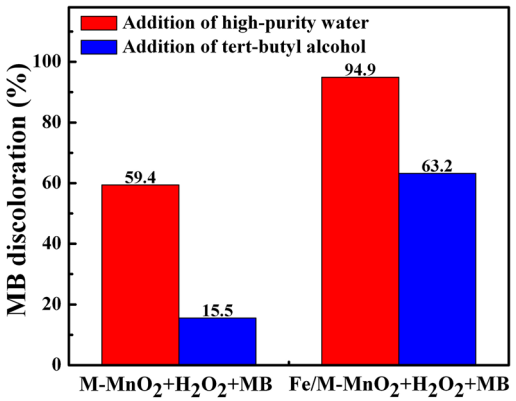

Figure 7. Effect of *tert*-butyl alcohol additions on MB degradation. Error bar = 0.3%.

An improved adsorption−oxidation−desorption mechanism is proposed. First, the MB molecules and H_2O_2 are adsorbed on the surface of the urchinlike MnO_2 hollow submicrospheres. Second, H_2O_2 is decomposed by the highly active catalyst. The H_2O_2 decomposition in the M-MnO_2 + H_2O_2 + MB system is summarized in eqs 1 and 2 according to previous literature:[9,55]

$$H_2O_2 \xrightarrow{MnO_2} H_2O + O_2 \quad (1)$$

$$H_2O_2 \xrightarrow{MnO_2} 2\cdot OH \quad (2)$$

The main reaction, eq 1, is very rapid, and most O_2 escapes from the reaction medium instead of participating in the reaction: R−H + O_2 → R· + HO_2· (R−H is organic matter). However, the secondary reaction, eq 2, is very slow so only a small production rate of free radicals is obtained. According to previous reports on catalytic decomposition of hydrogen peroxide on iron oxides,[15,56]

$$H_2O_2 + \equiv Fe^{3+} \rightarrow HO_2\cdot + H^+ + \equiv Fe^{2+}$$

$$H_2O_2 + \equiv Fe^{2+} \rightarrow \cdot OH + \equiv Fe^{3+} + OH^-$$

Fe substitution in Fe/M-MnO_2 can clearly increase the rate constant of reaction 2 and urge H_2O_2 to produce more free radicals for MB degradation, leading to the enhancement of catalytic activity of M-MnO_2.

The nascent free radical species have high oxidizing ability and can cause destructive oxidation of refractory organic

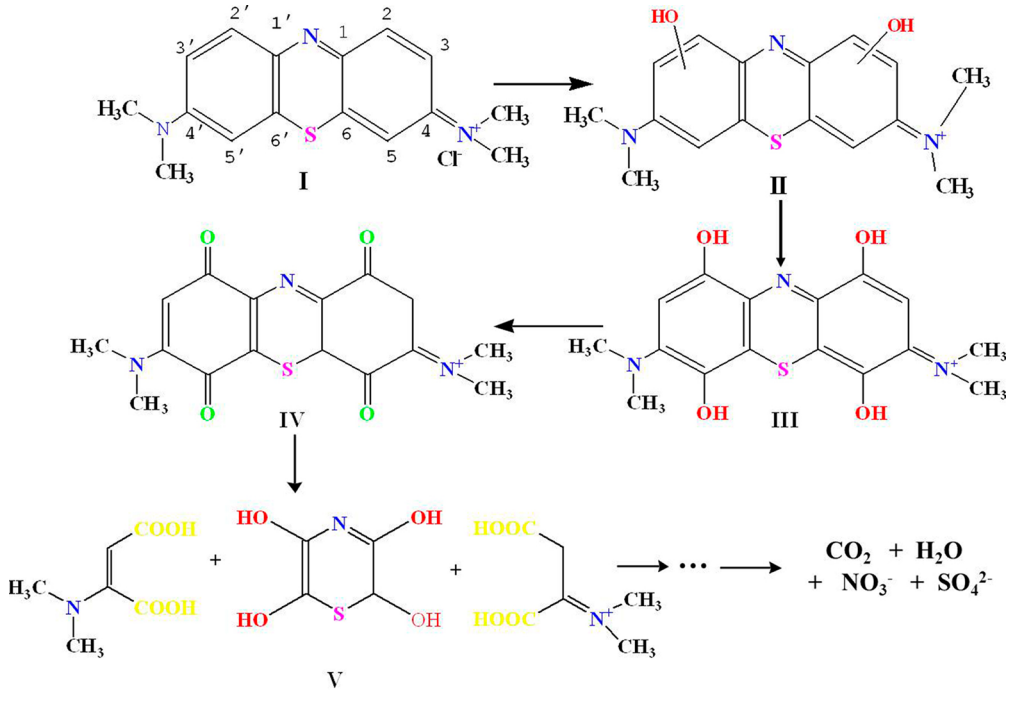

Figure 8. A possible degradation path for MB in the Fe/M-MnO_2 + H_2O_2 + MB system.

DOI: 10.1021/am505989j
ACS Appl. Mater. Interfaces 2015, 7, 3949−3959

pollutants.[2,57,58] The reactions of free radicals in MB degradation can be summarized in the following sequential equations:

$$R{-}H + \cdot OH \rightarrow R\cdot + H_2O$$

$$R\cdot + O_2 \rightarrow ROO\cdot$$

$$ROO\cdot(R'C(O)O) \rightarrow R'\cdot + CO_2$$

As a result, R−H would be destructed by free radicals to produce smaller organic compounds. To provide further insight into the degradation intermediates of MB, the MB solution and filtered solutions (C1 and C2, see the Supporting Information) were investigated by FTIR spectroscopy (Figure S5, Supporting Information). As shown in the spectrum of the initial MB solution, the peak at 1385 cm^{-1} represents the C−N stretching vibration of $-N-(CH_3)_2$. Four small peaks located at 1450, 1500, 1580, and 1605 cm^{-1} correspond to bending vibrations of the benzene ring. The results originate from the characteristic molecular structure of MB. The broad peak at 3448 cm^{-1} is due to the presence of the ·OH group of an adsorbed water molecule. The spectrum of C1 verifies that the intensities of the characteristic peaks of MB decline and new small peaks arise around 1700−1720 cm^{-1}, indicating the presence of remnant MB and the appearance of a C═O vibration in some carboxylic acid, aldehydes, or ketones. The M-MnO_2 + H_2O_2 + MB system has realized the preliminary conversion of MB. The spectrum of C2 has no characteristic absorption peaks of a benzene ring, $-CH_3$ (three characteristic peaks at 1450, 2692, and 2872 cm^{-1}), and C−N, but there are new peaks located at 585, 856, 1006, and 1068 cm^{-1}. The peaks around 856 imply the presence of a NO_3^- or C−O vibration of a carboxylic acid, while the peaks in the range of 1000−1200 cm^{-1} result from the C−O stretching vibration of alcohol or ether. The above results suggest that the benzene ring of MB in the Fe/M-MnO_2 + H_2O_2 + MB system is destroyed and intermediates with smaller molecular weights such as carboxylic acids and alcohols are formed instead of complete mineralization.

A similar conclusion is obtained from the FTIR spectra,[9] ESI-MS trap mass spectroscopy,[47,51] HPLC,[58] or HPLC-MS[49] in the CWPO of refractory organic pollutants. Oliveira et al. proposed the degradation path of MB by calculation of the Gibbs free energy of the intermediates.[47,50] Their study indicates that MB is transformed into small organic compounds at first and then further degrades into CO_2 and H_2O. So a possible degradation path for the CWPO of MB is deduced according to FTIR analysis and previous reports.[50,57] Due to strong oxidizing capacity and the electrophilic addition property of ·OH, the ·OH initially attacks the benzene ring, having a higher electron density, in the reaction with aromatic compounds.[57,59] Rearrangement of covalent bonds can occur in the aromatic ring system. Usually, a 1,2- or 1,5-hydrogen atom transfer occurs to form the benzoquinone structure as shown in Figure 8 (IV). This benzoquinone structure is very unstable; the C−C chemical bond near the carbonyl is destructed by ·OH to produce −COOH or ROO· as shown in Figure 8 (V). Thus, the main intermediates from MB degradation are carboxylic acids such as butenedioic acid. These intermediates would be oxidized persistently by free radicals. When the dosage of H_2O_2 is too small to completely mineralize aromatic compounds, MB would havd priority for removal, and the degradation reaction would go to the end in the acid production phase. Although these new insights obtained in this study are beneficial for constructing the degradation mechanism for MB, further investigation on the reaction mechanism of the catalytic wet hydrogen peroxide oxidation process is necessary.

4. CONCLUSIONS

In summary, a novel catalyst, Fe-species-loaded mesoporous manganese dioxide (Fe/M-MnO_2) urchinlike superstructures, has been successfully prepared for the degradation of organic contaminants in wastewater via a heterogeneous Fenton mechanism. The hierarchical M-MnO_2 urchinlike superstructures have been first synthesized by means of a facile and environmental friendly method on a soft interface between CH_2Cl_2 and H_2O without templates. The hierarchical urchinlike superstructure consists of ε-MnO_2 hollow submicrospheres with size ranges from 200 to 500 nm. The average pore diameter, mesoporous volume, and specific surface area are respectively 5.87 nm, 0.451 $cm^3\cdot g^{-1}$, and 219.3 $m^2\cdot g^{-1}$. The M-MnO_2-supported Fe catalysts (Fe/M-MnO_2) have been fabricated through incipient wetness impregnation and calcination. EDX microanalysis indicates the availability of Fe loading processes and the homogeneity of Fe in Fe/M-MnO_2. The specific surface area, pore volume, and average pore diameter of Fe/M-MnO_2 are 129.1 $m^2\cdot g^{-1}$, 0.355 $cm^3\cdot g^{-1}$, and 6.85 nm, respectively. Compared with M-MnO_2, the catalytic performance of Fe/M-MnO_2 is much better, with an increase of 23% in the degradation of MB, and exhibits excellent performance in the catalytic wet hydrogen peroxide oxidation of MB. When the reaction was conducted for 120 min, ca. 94.8% of MB was decomposed. The consumption of MB caused by 1 g of catalyst and 1 L of 30 wt % H_2O_2 solution could reach up to 18.9 g. In contrast to iron oxide dispersed into other supports, the highlight of Fe/M-MnO_2 is that the H_2O_2 decomposition and MB degradation are both very rapid. The remarkable stability of this Fe/M-MnO_2 catalyst in the reaction medium has been confirmed by the iron leaching test and reuse experiments. Mechanism analysis revealed that the hydroxyl free radical (·OH) is mainly responsible for the removal of MB in the heterogeneous catalytic system catalyzed by M-MnO_2 and Fe/M-MnO_2. MB is transformed into small organic compounds and then is further degraded into CO_2 and H_2O. The new insights obtained in this study are beneficial for the practical applications of heterogeneous catalysts in wastewater treatments.

■ ASSOCIATED CONTENT

Supporting Information

Chemicals used, catalyst characterizations, catalytic performances of filtered solutions in this study, XRD patterns, FTIR spectra, SEM images, and porous properties of M-MnO_2 and Fe/M-MnO_2 samples, UV−vis absorption and FTIR spectra of MB solution, and chemical structure of MB. This material is available free of charge via the Internet at http://pubs.acs.org.

■ AUTHOR INFORMATION

Corresponding Authors

*Phone: +86 21 66137503. Fax: +86 21 66137787. E-mail: zwchen@shu.edu.cn.
*E-mail: mhwu@staff.shu.edu.cn.
*E-mail: apcmlwu@cityu.edu.hk.

Notes

The authors declare no competing financial interest.

DOI: 10.1021/am505989j
ACS Appl. Mater. Interfaces 2015, 7, 3949−3959

■ ACKNOWLEDGMENTS

The work described in this article was financially supported by the National Natural Science Foundation of China (project numbers: 11375111, 11428410, 11074161, 11025526, 41373098, and 41430644), the Research Fund for the Doctoral Program of Higher Education of China (project number: 20133108110021), the Key Innovation Fund of Shanghai Municipal Education Commission (project numbers: 14ZZ098 and 10ZZ64), the Science and Technology Commission of Shanghai Municipality (project numbers: 14JC1402000 and 10JC1405400), the Shanghai Pujiang Program (project number: 10PJ1404100), and the Program for Changjiang Scholars and Innovative Research Team in University (project number: IRT13078). This work was also supported by a grant from the Research Grants Council of the Hong Kong Special Administrative Region, China [project no. (RGC ref. No.), CityU 119212].

■ REFERENCES

(1) Peng, X. S.; Ichinose, I. Manganese Oxyhydroxide and Oxide Nanofibers for High Efficiency Degradation of Organic Pollutants. *Nanotechnology* **2011**, *22*, 015701−1−7.

(2) Zhang, W. X.; Yang, Z. H.; Wang, X.; Zhang, Y. C.; Wen, X. G.; Yang, S. H. Large-Scale Synthesis of β-MnO_2 Nanorods and Their Rapid and Efficient Catalytic Oxidation of Methylene Blue Dye. *Catal. Commun.* **2006**, 408−412.

(3) Zhang, L.; Zhou, X. Y.; Guo, X. J.; Song, X. Y.; Liu, X. Y. Investigation on the Degradation of Acid Fuchsin Induced Oxidation by $MgFe_2O_4$ under Microwave Irradiation. *J. Mol. Catal. A* **2011**, *335*, 31−37.

(4) Kannan, R.; Peera, S. G.; Obadiah, A.; Vasanthkumar, S. MnO_2 Supported POM-A Novel Nanocomposite for Dye Degradation. *Dig. J. Nanomater. Biostruct.* **2011**, *6*, 829−835.

(5) Gupta, V. K. Suhas. Application of Low-Cost Adsorbents for Dye Removal-A Review. *J. Environ. Manage.* **2009**, *90*, 2313−2342.

(6) Slokar, Y. M.; Le Marechal, A. M. Methods of Decoloration of Textile Wastewaters. *Dyes Pigm.* **1998**, *37*, 335−356.

(7) Chen, C. C.; Liao, H. J.; Cheng, C. Y.; Yen, C. Y.; Chung, Y. C. Biodegradation of Crystal Violet by Pseudomonas Putida. *Biotechnol. Lett.* **2007**, *29*, 391−396.

(8) Wang, J. L.; Xu, L. J. Advanced Oxidation Processes for Wastewater Treatment: Formation of Hydroxyl Radical and Application. *Crit. Rev. Environ. Sci. Technol.* **2012**, *42*, 251−325.

(9) Zhang, L. L.; Nie, Y. L.; Hu, C.; Hu, X. X. Decolorization of Methylene Blue in Layered Manganese Oxide Suspension with H_2O_2. *J. Hazard. Mater.* **2011**, *190*, 780−785.

(10) Neyens, E.; Baeyens, J. A Review of Classic Fenton's Peroxidation as an Advanced Oxidation Technique. *J. Hazard. Mater.* **2003**, *98*, 33−50.

(11) Rhadfi, T.; Piquemal, J. Y.; Sicard, L.; Herbst, F.; Briot, E.; Benedetti, M.; Atlasani, A. Polyol-Made Mn_3O_4 Nanocrystals as Efficient Fenton-Like Catalysts. *Appl. Catal., A* **2010**, 132−139.

(12) Lim, H.; Lee, J.; Jin, S.; Kim, J.; Yoon, J.; Hyeon, T. Highly Active Heterogeneous Fenton Catalyst Using Iron Oxide Nanoparticles Immobilized in Alumina Coated Mesoporous Silica. *Chem. Commum.* **2006**, 463−465.

(13) Guimaraes, I. R.; Oliveira, L.; Queiroz, P. F.; Ramalho, T. C.; Pereira, M.; Fabris, J. D.; Ardisson, J. D. Modified Goethites as Catalyst for Oxidation of Quinoline: Evidence of Heterogeneous Fenton Process. *Appl. Catal., A* **2008**, *347*, 89−93.

(14) Gregor, C.; Hermanek, M.; Jancik, D.; Pechousek, J.; Filip, J.; Hrbac, J.; Zboril, R. The Effect of Surface Area and Crystal Structure on the Catalytic Efficiency of Iron(III) Oxide Nanoparticles in Hydrogen Peroxide Decomposition. *Eur. J. Inorg. Chem.* **2010**, 2343−2351.

(15) Pham, A.; Lee, C.; Doyle, F. M.; Sedlak, D. L. A Silica-Supported Iron Oxide Catalyst Capable of Activating Hydrogen Peroxide at Neutral pH Values. *Environ. Sci. Technol.* **2009**, *43*, 8930−8935.

(16) Cornu, C.; Bonardet, J. L.; Casale, S.; Davidson, A.; Abramson, S.; Andre, G.; Porcher, F.; Grcic, I.; Tomasic, V.; Vujevic, D.; Koprivanac, N. Identification and Location of Iron Species in Fe/SBA-15 Catalysts: Interest for Catalytic Fenton Reactions. *J. Phys. Chem. C* **2012**, *116*, 3437−3448.

(17) Iurascu, B.; Siminiceanu, I.; Vione, D.; Vicente, M. A.; Gil, A. Phenol Degradation in Water through A Heterogeneous Photo-Fenton Process Catalyzed by Fe-Treated Laponite. *Water Res.* **2009**, *43*, 1313−1322.

(18) Lee, Y. C.; Chang, S. J.; Choi, M. H.; Jeon, T. J.; Ryu, T.; Huh, Y. S. Self-Assembled Graphene Oxide with Organo-Building Blocks of Fe-Aminoclay for Heterogeneous Fenton-Like Reaction at Near Neutral pH: A Batch Experiment. *Appl. Catal., B* **2013**, *142*, 494−503.

(19) Ramirez, J. H.; Maldonado-Hodar, F. J.; Perez-Cadenas, A. F.; Moreno-Castilla, C.; Costa, C. A.; Madeira, L. M. Azo-Dye Orange II Degradation by Heterogeneous Fenton-Like Reaction Using Carbon-Fe Catalysts. *Appl. Catal., B* **2007**, *75*, 312−323.

(20) Xu, C. B.; Teja, A. S. Characteristics of Iron Oxide/Activated Carbon Nanocomposites Prepared Using Supercritical Water. *Appl. Catal., A* **2008**, *348*, 251−256.

(21) Kasiri, M. B.; Aleboyeh, H.; Aleboyeh, A. Degradation of Acid Blue 74 Using Fe-ZSM5 Zeolite as a Heterogeneous Photo-Fenton Catalyst. *Appl. Catal., B* **2008**, *84*, 9−15.

(22) Sui, N.; Duan, Y. Z.; Jiao, X. L.; Chen, D. R. Large-Scale Preparation and Catalytic Properties of One-Dimensional α/β-MnO_2 Nanostructures. *J. Phys. Chem. C* **2009**, *113*, 8560−8565.

(23) Chen, Y. C.; Duan, Z. Y.; Min, Y. L.; Shao, M. W.; Zhao, Y. G. Synthesis, Characterization and Catalytic Property of Manganese Dioxide with Different Structures. *J. Mater. Sci.* **2011**, *22*, 1162−1167.

(24) Zhang, Y. G.; Chen, L. Y.; Zheng, Z.; Yang, F. L. A Redox-Hydrothermal Route to β-MnO_2 Hollow Octahedra. *Solid State Sci.* **2009**, *11*, 1265−1269.

(25) Yang, Z. H.; Zhang, Y. C.; Zhang, W. X.; Wang, X.; Qian, Y. T.; Wen, X. G.; Yang, S. H. Nanorods of Manganese Oxides: Synthesis, Characterization and Catalytic Application. *J. Solid State Chem.* **2006**, *179*, 679−684.

(26) Tian, Z. R.; Tong, W.; Wang, J. Y.; Duan, N. G.; Krishnan, V. V.; Suib, S. L. Manganese Oxide Mesoporous Structures: Mixed-Valent Semiconducting Catalysts. *Science* **1997**, *276*, 926−930.

(27) Li, L. X.; Hua, P.; Tian, X. K.; Yang, C.; Pi, Z. B. Synthesis and Electrochemical Properties of Two Types of Highly Ordered Mesoporous MnO_2. *Electrochim. Acta* **2010**, *55*, 1682−1686.

(28) Kim, J. M.; Huh, Y. S.; Han, Y. K.; Cho, M. S.; Kim, H. J. Facile Synthesis Route to Highly Crystalline Mesoporous Gamma-MnO_2 Nanospheres. *Electrochem. Commun.* **2012**, *14*, 32−35.

(29) Yuan, C. Z.; Gao, B.; Su, L. H.; Zhang, X. G. Interface Synthesis of Mesoporous MnO_2 and Its Electrochemical Capacitive Behaviors. *J. Colloid Interface Sci.* **2008**, *322*, 545−550.

(30) Liu, M.; Zhang, G. J.; Shen, Z. R.; Sun, P. C.; Ding, D. T.; Chen, T. H. Synthesis and Characterization of Hierarchically Structured Mesoporous MnO_2 and Mn_2O_3. *Solid State Sci.* **2009**, *11*, 118−128.

(31) Yuan, C. Z.; Hou, L. R.; Yang, L.; Li, D. K.; Shen, L. F.; Zhang, F.; Zhang, X. G. Facile Interfacial Synthesis of Flower-Like Hierarchical α-MnO_2 Sub-Microspherical Superstructures Constructed by Two-Dimension Mesoporous Nanosheets and Their Application in Electrochemical Capacitors. *J. Mater. Chem.* **2011**, *21*, 16035−16041.

(32) Liang, X. L.; Zhong, Y. H.; He, H. P.; Yuan, P.; Zhu, J. X.; Zhu, S. Y.; Jiang, Z. The Application of Chromium Substituted Magnetite as Heterogeneous Fenton Catalyst for the Degradation of Aqueous Cationic and Anionic Dyes. *Chem. Eng. J.* **2012**, *191*, 177−184.

(33) Zhang, X. J.; Liu, Y.; Liu, G. Q.; Tao, K.; Jin, Q.; Meng, F. Z.; Wang, D.; Tsubaki, N. Product Distributions Including Hydrocarbon and Oxygenates of Fischer−Tropsch Synthesis over Mesoporous MnO_2-Supported Fe Catalyst. *Fuel* **2012**, *92*, 122−129.

(34) Bai, Z. C.; Sun, B.; Fan, N.; Ju, Z. C.; Li, M. H.; Xu, L. Q.; Qian, Y. T. Branched Mesoporous Mn_3O_4 Nanorods: Facile Synthesis and

DOI: 10.1021/am505989j
ACS Appl. Mater. Interfaces 2015, 7, 3949−3959

Catalysis in the Degradation of Methylene Blue. *Chem.—Eur. J.* **2012**, *18*, 5319−5324.
(35) Dubal, D. P.; Kim, W. B.; Lokhande, C. D. Galvanostatically Deposited Fe: MnO_2 Electrodes for Supercapacitor Application. *J. Phys. Chem. Solids* **2012**, *73*, 18−24.
(36) Dubal, D. P.; Lokhande, C. D. Significant Improvement in the Electrochemical Performances of Nano-Nest Like Amorphous MnO_2 Electrodes Due to Fe Doping. *Ceram. Int.* **2013**, *39*, 415−423.
(37) Pokroy, B.; Aichmayer, B.; Schenk, A. S.; Haimov, B.; Kang, S. H.; Fratzl, P.; Aizenberg, J. Sonication-Assisted Synthesis of Large, High-Quality Mercury Thiolate Single Crystals Directly from Liquid Mercury. *J. Am. Chem. Soc.* **2010**, *132*, 14355−14357.
(38) Huang, W.; Lin, Y.; Taylor, S.; Gaillard, J.; Rao, A. M.; Sun, Y. P. Sonication-Assisted Functionalization and Solubilization of Carbon Nanotubes. *Nano Lett.* **2002**, *2*, 231−234.
(39) Polyakova (Stolyarova), E.; Rim, K. T.; Eom, D.; Douglass, K.; Opila, R. L.; Heinz, T. F.; Teplyakov, A. V.; Flynn, G. W. Scanning Tunneling Microscopy and X-ray Photoelectron Spectroscopy Studies of Graphene Films Prepared by Sonication-Assisted Dispersion. *ACS Nano* **2011**, *5*, 6102−6108.
(40) Xie, Y.; Ali, G.; Yoo, S. H.; Cho, S. O. Sonication-Assisted Synthesis of CdS Quantum-Dot-Sensitized TiO_2 Nanotube Arrays with Enhanced Photoelectrochemical and Photocatalytic Activity. *ACS Appl. Mater. Interfaces* **2010**, *2*, 2910−2914.
(41) Wu, S. H.; Wu, J. L.; Jia, S. Y.; Chang, Q. W.; Ren, H. T.; Liu, Y. Cobalt(II) Phthalocyanine-Sensitized Hollow Fe_3O_4@SiO_2@TiO_2 Hierarchical Nanostructures: Fabrication and Enhanced Photocatalytic Properties. *Appl. Surf. Sci.* **2013**, *287*, 389−396.
(42) Chen, H. M.; He, J. H. Facile Synthesis of Monodisperse Manganese Oxide Nanostructures and Their Application in Water Treatment. *J. Phys. Chem. C* **2008**, *112*, 17540−17545.
(43) Martinez, F.; Calleja, G.; Melero, J. A.; Molina, R. Iron Species Incorporated over Different Silica Supports for the Heterogeneous Photo-Fenton Oxidation of Phenol. *Appl. Catal., B* **2007**, *70*, 452−460.
(44) Pierotti, R. A.; Rouquerol, J. Reporting Physisorption Data for Gas/Solid Systems with Special Reference to the Determination of Surface Area and Porosity. *Pure Appl. Chem.* **1985**, *57*, 603−619.
(45) Ai, L. H.; Yue, H. T.; Jiang, J. Sacrificial Template-Directed Synthesis of Mesoporous Manganese Oxide Architectures with Superior Performance for Organic Dye Adsorption. *Nanoscale* **2012**, *4*, 5401−5408.
(46) Vinu, A.; Sawant, D. P.; Ariga, K.; Hossain, K. Z.; Halligudi, S. B.; Hartmann, M.; Nomura, M. Direct Synthesis of Well-Ordered and Unusually Reactive Fe/SBA-15 Mesoporous Molecular Sieves. *Chem. Mater.* **2005**, *17*, 5339−5345.
(47) Castro, C. S.; Guerreiro, M. C.; Oliveira, L. C. A.; Goncalves, M.; Anastacio, A. S.; Nazzarro, M. Iron Oxide Dispersed over Activated Carbon: Support Influence on the Oxidation of the Model Molecule Methylene Blue. *Appl. Catal., A* **2009**, *367*, 53−58.
(48) Yang, S. J.; He, H. P.; Wu, D. Q.; Chen, D.; Ma, Y. H.; Li, X. L.; Zhu, J. X.; Yuan, P. Degradation of Methylene Blue by Heterogeneous Fenton Reaction Using Titanomagnetite at Neutral pH Values: Process and Affecting Factors. *Ind. Eng. Chem. Res.* **2009**, *48*, 9915−9921.
(49) Zaied, M.; Peulon, S.; Bellakhal, N.; Desmazieres, B.; Chausse, A. Studies of N-Demethylation Oxidative and Degradation of Methylene Blue by Thin Layers of Birnessite Electrodeposited onto SnO_2. *Appl. Catal., B* **2011**, *101*, 441−450.
(50) Oliveira, L.; Goncalves, M.; Guerreiro, M. C.; Ramalho, T. C.; Fabris, J. D.; Pereira, M. C.; Sapag, K. A New Catalyst Material Based on Niobia/Iron Oxide Composite on the Oxidation of Organic Contaminants in Water via Heterogeneous Fenton Mechanisms. *Appl. Catal., A* **2007**, *316*, 117−124.
(51) Kuan, W. H.; Chen, C. Y.; Hu, C. Y.; Tzou, Y. M. Kinetic Modeling for Microwave-Enhanced Degradation of Methylene Blue Using Manganese Oxide. *Int. J. Photoenergy* **2013**, 849−916.
(52) Molina, R.; Martinez, F.; Melero, J. A.; Bremner, D. H.; Chakinala, A. G. Mineralization of Phenol by a Heterogeneous Ultrasound/Fe-SBA-15/H_2O_2 Process: Multivariate Study by Factorial Design of Experiments. *Appl. Catal., B* **2006**, *66*, 198−207.
(53) Anipsitakis, G. P.; Dionysiou, D. D. Radical Generation by the Interaction of Transition Metals with Common Oxidants. *Environ. Sci. Technol.* **2004**, *38*, 3705−3712.
(54) Xing, S. T.; Hu, C.; Qu, J. H.; He, H.; Yang, M. Characterization and Reactivity of MnO_x Supported on Mesoporous Zirconia for Herbicide 2,4-D Mineralization with Ozone. *Environ. Sci. Technol.* **2008**, *42*, 3363−3368.
(55) Do, S. H.; Batchelor, B.; Lee, H. K.; Kong, S. H. Hydrogen Peroxide Decomposition on Manganese Oxide (Pyrolusite): Kinetics, Intermediates, and Mechanism. *Chemosphere* **2009**, *75*, 8−12.
(56) Lin, S. S.; Gurol, M. D. Catalytic Decomposition of Hydrogen Peroxide on Iron Oxide: Kinetics, Mechanism, and Implications. *Environ. Sci. Technol.* **1998**, *32*, 1417−1423.
(57) Fukushima, M.; Tatsumi, K.; Morimoto, K. The Fate of Aniline after a Photo-Fenton Reaction in an Aqueous System Containing Iron(III), Humic Acid, and Hydrogen Peroxide. *Environ. Sci. Technol.* **2000**, *34*, 2006−2013.
(58) Zhang, S. X.; Zhao, X. L.; Niu, H. Y.; Shi, Y. L.; Cai, Y. Q.; Jiang, G. B. Superparamagnetic Fe_3O_4 Nanoparticles as Catalysts for the Catalytic Oxidation of Phenolic and Aniline Compounds. *J. Hazard. Mater.* **2009**, *167*, 560−566.
(59) Chen, L. Q.; Zhang, Y. G. Phenol Degradation by MnO_2 Assisted Fenton Reagent Oxidation Technology. *Chin. J. Environ. Eng.* **2012**, *6*, 4047−4052.

DOI: 10.1021/am505989j
ACS Appl. Mater. Interfaces 2015, 7, 3949−3959